RSC Advances

ROYAL SOCIETY OF CHEMISTRY

www.rsc.org/advances

Synthesis, biological evaluation and molecular modeling of 1*H*-benzo[*d*]imidazole derivatives as novel anti-tubulin polymerization agents

*Fang Wang, Xue Wang, Min-Xia Zhang, Yong-Hua Yang*and Hai-Liang Zhu**

State Key Laboratory of Pharmaceutical Biotechnology, Nanjing University, Nanjing 210093, People's Republic of China

* *Corresponding authors. Tel.: +86 25 89682572; Fax: +86 25 89682672.*

E-mail address: zhuhl@nju.edu.cn (H.-L. Zhu).

Abstract:

A series of novel compounds (**8a-21b**) were designed and synthesized based on 1*H*-benzo[*d*]imidazole. Their biological activities were evaluated as potential tubulin polymerization inhibitors and anticancer agents. Among all the compounds, compound **18b** showed the most potent *in vitro* growth inhibitory activity against A549, MCF-7, K562 cancer cell lines, with IC_{50} values of 0.12 μM, 0.15 μM, 0.21 μM, respectively. And, compound **18b** also exhibited significant tubulin polymerization inhibitory activity (IC_{50}=2.1 μM), which was comparable with the positive control. Furthermore, docking simulation and 3D-QSAR modeling of inhibitor analogues provide determination of the probable binding model and an important basis that compound **18b** with potent inhibitory activity in tumor growth may be a potential anticancer agent.

Keywords:

1*H*-benzo[*d*]imidazole

Anticancer activity

Tubulin inhibition

Molecular docking

1. Introduction

Cancer remains the most major cause of death in developed countries.[1, 2].Actually, the inducement of cancer is greatly complicated, involving many molecular mechanisms. Out of control in cell replication is one of the most important mechanisms that cause cancer.[3] Microtubules play a significant role during the process of cell replication. Mitotic spindle is formed by microtubule polymerization and fasten to the kinetochore of chromosomes when microtubules extend from the cell centrosome during cell mitosis.[4, 5] Therefore, the inhibition of microtubule polymerization has become to be the mode of action for several clinically successful anticancer drugs.[6] Tubulin is the major protein component of microtubules, and is becoming the target of more and more antimitotic drugs.

Colchicine (**Fig. 1**, **1a**) is the first natural highly effective drug that is demonstrated to bind to tubulin, interfering with microtubule polymerization, inducing cell cycle arrest, leading to cell death, [7, 8] and its binding site on tubulin has been characterized already.[9, 10] Among the naturally occurring compounds, podophyllotoxin (**Fig. 1**, **2b**), an antineoplastic and antiviral cytotoxic product, isolated from *Podophyllum spp* and several species of other genus and families, can strongly inhibit the polymerization of tubulin by binding to the colchicine binding site resulting in strong cytotoxicity against multiple human tumor.[11] In spite of its initial potentiality as an anticancer drug, human clinical trials were soon abandoned due to its toxicity and severe adverse effects.[12] However, an extensive program of structure-activity of podophyllotoxin has been conducted. Continuous efforts on podophyllotoxin modification led to the synthesis and development of several related compounds, as compounds **c1-c3** (**Fig. 1**, **c1**, **c2**, **c3**).[13] From the mechanistic point of view, it has been demonstrated that podophyllotoxin and its derivatives (**c1-c3**), act by very well inhibiting tubulin polymerization through interaction at the colchicine binding site.[14,15] Unfortunately, despite the intensive efforts focused on obtaining better derivatives or analogs, no substance of this family has been found that could outperform the efficacy of

podophyllotoxin (**1a**) and deoxypodophyllotoxin (**c1**) for inhibiting microtubule assembly.[16] So, further study required.

1*H*-benzo[*d*]imidazole is reported to be a very good basic skeleton that has gained prominence by exhibiting a wide variety of biological activities as well as producing useful intermediates in several organic preparations.[17, 18] 1*H*-benzo[*d*]imidazole derivatives have been reported to be anticancer, [19] anti-tubercular, [20]antimicrobial and analgesic.[21, 22] The action of 1*H*-benzo[*d*]imidazole connected with the apoptotic mechanisms and angiogenesis, which is a crucial step in the tumorigenesis seems to be very promising in anticancer therapy.[23, 24] What's more, some novel 1*H*-benzo[*d*]imidazole derivatives have been well designed and found to be differentiating inducers of human cancer cells, such as compound **d1** ((**Fig. 1**, **d1**), with IC_{50} value of 120-200 nM against A549 cell lines.[25] And there are a great quantity of evidences, derived from molecular modeling studies and experimental data, demonstrating how this class of inhibitors bind to the active site of tubulin.[26]

Therefore, due to these previous researches, in order to develop more potent tubulin inhibitor as antitumor agent, we attempt to use the 1*H*-benzo[*d*]imidazole as the basic scaffold for the design of a series of novel tubulin polymerization inhibitors. We try to integrate the substructure benzo[*d*][1,3]dioxole of podophyllotoxin with 1*H*-benzo[*d*]imidazole to screen new basic scaffold((**Fig. 1**, **e1**). The two combined substructures might exhibit synergistic effect in anticancer activities. In order to extend our research and to gain further insight in their structure–activity relationships (SARs), we search more novel agents to inhibit tubulin polymerization. Thus, our strategy for further development of active antimitotic agents was to perform modifications on the three aromatic ring (A, B, C ring), once the new combined scaffold was identified as the minimum structural requirement for activity in this new series of compounds. Then some substituents was introduced onto the three aromatic rings, and the modifications have been performed to screen a series of active anti-tubulin agents.

In this paper, we discussed the synthetic method of this series of compounds, evaluated their anticancer and anti-tubulin activities, learned the influence on cell

apoptosis, and analyzed the structure–activity relationship. The docking study based on tubulin crystal structure (PDB code: 1SAO) showed compounds **18b**, **19a** and **15a** exhibit more affinity for tubulin than colchicine, which rationally proved the reason why these compounds also possess effective inhibitory activity profile against tubulin. Additionally, 3D-QSAR model provided more information that could be applied to design new molecules with more potent tubulin inhibitory activity

2. Results and discussion

2.1. Chemistry

The synthetic routes for the novel 1*H*-benzo[*d*]imidazole derivatives **8a–14b** and **9a-21b** are outlined respectively in **Scheme 1** and **Scheme 2**. These compounds **8a-14b** were synthesized from 2-(benzo[*d*][1,3]dioxol-5-yl)-1*H*-benzo[*d*]imidazoles **8-14** and substituted 2-chloro-1,3-dinitro-5-(trifluoromethyl)benzene **a-b**. First of all, 3,4-dihydroxybenzaldehyde was dissolved in cool acetonitrile(CH_3CN), then K_2CO_3 was added , with that dibromomethane was added dropwise. The reaction mixture was then stirred at 90 ℃ for 24 h, and benzo[*d*][1,3]dioxole-5-carbaldehyde **2a** were obtained. Secondly, **2a** and substituted benzene-1,2-diamine **1-7** were dissolved in cool DMF, with that $Na_2S_2O_5$ was added. The reaction mixture was then stirred at 90 ℃ for 4-6 h, and compounds **8-14** were gained. At last, compounds **8-14** and substituted 2-chloro-1,3-dinitro-5-(trifluoromethyl)benzene **a-b** were dissolved in cool CH_3CN , with that K_2CO_3 was added. The reaction mixture was then stirred at 90 ℃ for 12 h, and refluxed to give the desired compounds **8a–14b** (**Table 1**).

On the other hand, compounds **9a-21b** were synthesized from 2-(2,3-dihydrobenzo[*b*][1,4]dioxin-6-yl)-1*H*-benzo[*d*]imidazoles **15-21** and 2-chloro-1,3-dinitro-5-(trifluoromethyl)benzene **a-b**. To start, 3, 4-dihydroxybenzaldehyde was dissolved in cool CH_3CN, K_2CO_3 and 1,2-dibromoethane were added to give 2,3-dihydrobenzo[*b*][1,4]dioxine-6-carbaldehyde **2b**, then , as the same way above that gained compounds **8a-14b** to get compounds **15a–21b** (**Table 2**). All of the

synthetic compounds **8a–21b** gave satisfactory elementary analytical and spectroscopic data. ^{1}H NMR, ^{13}C NMR and ESI-MS spectra were consistent with the assigned structures.

2.2. Crystal structure determination

Among them, a crystal structure of compound **8a** was determined by X-ray diffraction analysis. The crystal data presented in **Table 3** and **Fig. 2** give perspective views of **8a** in the form of trans-isomerism with the atomic labeling system.

2.3. Biological evaluation

2.3.1. *In vitro* anti-proliferative activities

We prepared three different human cancer cell lines including MCF-7 (human breast cancer cell line), A549 (human lung cancer cell), K562 (Human leukemia cells line) and 293T (as normal cell line) to test the anticancer activities of the synthesized compounds **8a-21b**. The results are summarized in **Table 4**. From the results, compound **18b** was found to be the most active among all compounds exhibiting IC_{50} values of 0.12 μM, 0.15 μM and 0.21 μM against A549, MCF-7 and k562 cell lines, respectively. Among all the 25 tested compounds, **8a**, **11b**, **15a**, **16a**, **18b**, **19b** and **20a** possessed the highest overall potency with substitute values of 0.12– 0.43 μM against all the three typical cancer cell lines. What's more, the results indicate these compounds possess highly safety.

Therefore, we could draw a conclusion that the activity of the tested compounds may be associated with the variation and modifications of the structure. The importance of substituents on C ring was demonstrated for activity and selectivity against the different cancer cell lines. Comparing with **11b** (C ring is five-membered ring), **18b** (C ring become to six-membered ring), has a higher activity. What's more, comparing **12b** and **19b**, **13a** and **20a**, **13b** and **20b**, **14a** and **21a**, compounds with six-membered ring have higher activity, respectively.

Among the compounds that substituted on A ring (all substituted on the same site), **15a**, **16a**, **16b**, **17a** (IC_{50}=0.19 μM, 0.31 μM, 0.49 μM, 0.66 μM) exhibited significant

anti-proliferative activities in the order of –H > -F > -Cl> -Br in MCF-7 cell line. And, **8a**, **9a**, **9b**, **10a** showed the similar order. For B ring, we use 2-chloro-1,3-dinitro-5-(trifluoromethyl)benzene and Chlorine-substituted 2-chloro-1,3-dinitro-5-(trifluoromethyl)benzene to modify. Comparing **11b** and **8a**, **12b** and **9a**, **13a** and **9b**, **13b** and **10a**, respectively, it is shown that compounds modified with Chlorine-substituted 2-chloro-1,3-dinitro-5-(trifluoromethyl)benzene have higher activity.

2.3.2. Inhibition of tubulin polymerization

To validate whether the above anti-proliferative effect was produced by interaction between tubulin and the synthesized compounds, the synthesized compounds were evaluated for their abilities to inhibit the tubulin polymerization. As expected, compound **18b** exhibited most potent anti-tubulin polymerization activity and the most of the activity data suggested that the IC_{50} values of these compounds showed a similar tendency as their relevant IC_{50} values in the anti-proliferative assay. Hence, a further study comparing the anti-proliferative activity of the top 10 compounds (**18b**, **15a**, 1**1b**, **16a**, **8a**, **20a**, **16b**, **17a**, **20b** and **12a**) against A549 cell line with the tubulin polymerization inhibitory activity was performed and the result indicated that there was a moderate correlation between tubulin polymerization inhibition and the inhibition of cancer cellular proliferation as evidenced in **Figure. 3** with an R^2 value of 0.9534. Therefore, we could get a summary that the synthesized molecule inhibitors can inhibit the tubulin polymerization and the anti-proliferative effect was produced partly by interaction between tubulin and the compounds.

2.3.3. Compound 18b induced apoptosis

In order to test whether the inhibition of cell growth of A549 was related to cell apoptosis, we performed a biparametric cytofluorimetric analysis using propidium iodide (PI) and annexin-V-FITC, which stain DNA and phosphatidylserine (PS) residues, respectively. A549 cells were treated with compound **18b** at 0.05 μM, 0.10 μM and 0.15 μM for 24 h, respectively, and DMSO served as a control. The results showed that the percentage of cell apoptosis was 3.58% at 0 μM for compound **18b**,

and cell apoptosis was increased to 5.80%, 13.14%, and 29.56% at 0.05 μM, 0.10 μM and 0.15 μM, respectively, (**Fig. 4**). Thus, compound **18b** could cause cell apoptosis like other tubulin-binding agents.

2.4. Computational

2.4.1. Molecular docking

Molecular docking is an application wherein molecular modeling techniques are used to predict how protein receptors interact with small molecules. Then, molecular docking of all the synthesized compounds into active binding site of tubulin was performed to simulate a binding mode derived from tubulin (PDB code: 1SAO). All docking runs were applied LigandFit Dock protocol of Discovery Studio 3.5.

The docking calculation of the synthesized compounds was showed in **Table5**. The interaction energy between compounds **8a-21b** and tubulin showed the corresponding results with tubulin polymerization inhibitory activity. Among the synthesized compounds, compound **18b** showed the lowest interaction energy. The binding modes of compound **18b** and tubulin were depicted in **Figure 5**. The amino acid residue which had interaction with tubulin was labeled in **Figure 5**A. In the binding mode, compound **18b** was nicely bound to the colchicine binding site of tubulin via one hydrogen bond, one π-cation interaction and two electrostatic interactions. The oxygen atom of two $-NO_2$ groups on B-ring of **18b** formed two electrostatic interactions with the amino of Lys B:254 and Lys B:352, respectively; Also B-ring of **18b** and the amino of Lys B: 254 formed one π-cation interaction (bond length: 5.91); What's more, the atom F of $-CF_3$ on B-ring of **18b** formed one hydrogen bond with amino hydrogen of CysB:241 (bond length: CysB:241 N – H. . .F = 2.06). This molecular docking results along with the biological assay data suggested that compound 18b was a potential inhibitor of tubulin.

2.4.1.1. 3D-QSAR model

To obtain a systematic SAR profile on 1*H*-benzo[*d*]imidazole derivatives as antitumor agents, to explore the more potent and selective tubulin inhibitors,

3D-QSAR model was built to select activity conformation of the designed molecular and reasonably evaluated the designed molecules by using the corresponding pIC_{50} values which were converted from the obtained IC_{50} (μM) values of tubulin inhibition (the way of this transformation was derived from an online calculator developed by an indian medicinal chemistry lab (http://www.sanjeevslab.org/tools-IC_{50}.html)) and performed by built-in QSAR software of DS 3.5 (Discovery Studio 3.5, Accelrys, Co. Ltd). The training and test sets were divided by the random diverse molecules method of DS 3.5, in which the training set accounted for 80% of all the molecules while the test set was set to 20%. The training set composes 20 agents and 5 agents were consisted of the relative test set. The graphical relationship of observed and predicted values were illustrated in **Figure 6**. In which the plot of the observed IC_{50} versus the predicted values showed that this model could be used in prediction of activity for 1*H*-benzo[*d*]imidazole derivatives. Also the molecules aligned with the iso-surfaces of the 3D-QSAR model coefficients on electrostatic potential grids (**Fig. 7**A) and Van der Waals grids (**Fig. 7**B) were listed. Electrostatic map indicated red contours around regions where high electron density (negative charge) was expected to increase activity, and blue contours represent areas where low electron density (partial positive charge) was expected to increase activity. Similarly, steric map indicated areas where steric bulk was predicted to increase (green) or decrease (yellow) activity. It was widely acceptable that a better inhibitor based on the 3D-QSAR model should have strong Van der Waals attraction in the green areas and a polar group in the blue electrostatic potential areas (which were dominant close to the skeleton). As expected, those potent compounds (**18b**, **15a**) not only could circumvent the red sub-region or the unfavorable yellow steric sub-region but also can get more close to the favorable blue and green spaces. Thus, this promising model would provide a guideline to design and optimize more effective tubulin inhibitors and pave the way for us in the further study.

3. Conclusion

In this paper, a series of novel compounds (**8a–21b**) bearing 1*H*-benzo[*d*]imidazole skeleton and the substructure benzo[*d*][1,3]dioxole of podophyllotoxin has been synthesized and evaluated as tubulin polymerization inhibitors. These compounds exhibited potent tubulin polymerization inhibitory activities and anti-proliferative activities against A549, MCF-7 and K562 cell lines. Compound **18b** showed the most potent anti-proliferative activity with an IC_{50} values of 0.12 μM, 0.15 μM and 2.10 μM against A549, MCF-7 and K562 cell lines, respectively, as well as tubulin polymerization inhibitory activity with an IC_{50} of 2.1 μM. Molecular docking and 3D-QSAR were further performed to study the inhibitor-tubulin protein interactions. According to the analysis of the binding model of compound **18b** with tubulin, several interactions were observed with the protein residues in the colchicine binding site might play a crucial role in its anti-tubulin polymerization and anti-proliferative activities. The research of these well designed compounds might be greatly helpful for the design and synthesis of tubulin polymerization inhibitors with better activities.

4. Experimental section

4.1. Materials and measurements

All reagents and solvents were of analysis or synthesis grade. ^{1}H NMR-spectra were recorded on a Bruker DPX300 model Spectrometer at 400 MHz, in DMSO-d_6 and chemical shifts were reported in ppm (d). TLC was performed on the glass backed silica gel sheets (Silica Gel 60 GF254) and visualized in UV light (254 nm and 365 nm). Column chromatography was performed using silica gel (200-300 mesh) eluting with ethyl acetate and petroleum ether. Melting points (uncorrected) were measured on a X-4 MP apparatus (Taike Corp, Beijing, China).

4.2. Synthesis

4.2.1. General procedure for synthesis of compound (2a)

A solution of 3,4-dihydroxybenzaldehyd (13.8 g, 100 mmol) in 200 mL cool acetonitrile (CH_3CN), were added K_2CO_3 (40 g), dibromomethane (120 mmol, 10.4 mL).The reaction mixture was then stirred at 90 ℃ for 24 h. After the reaction

completed, reaction mixture was filtered and concentrated, then the concentration was extracted with ethyl acetate and water. The combined extracts were dried with anhydrous Na_2SO_4 and concentrated. The pure white solid benzo[*d*][1,3]dioxole-5-carbaldehyde **2a** was gained with yield of 90%.

4.2.2. General procedure for synthesis of compounds (8-14)

A mixture of substituted benzene-1,2-diamine (1 mmol), $Na_2S_2O_5$ (1 mmol) and **2a** (1.2 mmol) were dissolved in DMF (10 mL) and stirred on 100 ℃ for 6 h. Reaction mixture poured into 500 mL water and filtered to give compounds **8-14** with yield of 72–81%.

4.2.3. General procedure for synthesis of compounds (8a-14b)

Compounds **8a-14b** were synthesized by coupling of substituted 2-chloro-1,3-dinitro-5-(trifluoromethyl)benzene **a-b** (1.2 mmol) with compounds **8-14** (1.0 mmol) using CH_3CN (20 mL) and K_2CO_3 (1.5 mmol). The reaction mixture was then stirred at 90 ℃ for 12 h. Then, filtered and concentrated, the residue was purified by column (200-300 mesh) chromatography using petroleum ether and ethyl acetate (8:1).

4.2.4. General procedure for synthesis of compound (2b)

To a solution of 3,4-dihydroxybenzaldehyd (13.8 g, 100 mmol) in 200 mL cool acetonitrile (CH_3CN), K_2CO_3 (40 g) and 1,2-dibromoethane (10 mL) were added. The reaction mixture was then stirred at 90 ℃ for 24 h. After the reaction completed, reaction mixture was filtered and concentrated, then the concentration was extracted with ethyl acetate and water. The combined extracts were dried with anhydrous Na_2SO_4 and concentrated to give 2,3-dihydrobenzo[*b*][1,4]dioxine-6-carbaldehyde **2b**, yield of 88%.

4.2.5. General procedure for synthesis of compounds (15-21)

A mixture of substituted benzene-1,2-diamine (1 mmol), $Na_2S_2O_5$ (1 mmol) and **2b** (1.2 mmol) were dissolved in DMF (10 mL) and stirred on 100 ℃ for 6 h. Reaction mixture poured into 500 mL water and filtered to give compounds **15-21** with yield of 71 – 83%.

4.2.6. General procedure for synthesis of compounds (15a-21b)

Compounds **15a-21b** were synthesized by coupling of substituted 2-chloro-1,3-dinitro-5-(trifluoromethyl)benzene (1.2 mmol) with compounds **15-21** (1.0 mmol) using CH_3CN (10 mL) and K_2CO_3 (1.5 mmol). The reaction mixture was then stirred at 90 ℃ for 12 h. Then, filtered and concentrated, the residue was purified by column (200-300 mesh) chromatography using petroleum ether and ethyl acetate (8:1).

4.3. Spectral properties of 1*H*-benzo[*d*]imidazole derivatives

4.3.1.2-(benzo[*d*][1,3]dioxol-5-yl)-1-(2,6-dinitro-4-(trifluoromethyl)phenyl)-1*H*-benzo[*d*]imidazole (8a)

Yellow powder, yield 81%. M p: 175-177 ℃. ^{1}H NMR (400 MHz, DMSO-d_6) δ : 9.07 (s, 2H,Ar-H), 7.81 (d, J = 8.0 Hz, 1H, Ar-H), 7.39-7.32 (m, 1H, Ar-H), 7.30 (d, J = 4.0 Hz, 2H, Ar-H), 7.11 (d, J = 1.6 Hz, 1H, Ar-H), 6.96 (d, J = 2.0 Hz, 1H, Ar-H), 6.92 (d, J = 8.0 Hz, 1H, Ar-H), 6.11 (s, 2H, CH_2). MS (ESI): 473.37 $[M+H]^+$. Anal. Calcd for $C_{21}H_{11}F_3N_4O_6$: C, 53.40; H, 2.35; N, 11.86. Found: C, 53.38; H, 2.32; N, 11.83.

4.3.2.2-(benzo[*d*][1,3]dioxol-5-yl)-1-(2,6-dinitro-4-(trifluoromethyl)phenyl)-5-methyl-1*H*-benzo[*d*]imidazole (8b)

Red powder, yield 71%. M p: 177-179℃. ^{1}H NMR (400 MHz, DMSO-d_6) δ: 9.05 (d, J = 4.4 Hz, 2H, Ar-H),7.67 (t, J = 32.0 Hz ,1H, Ar-H), 7.17 (t, J = 14.2 Hz, 1H, Ar-H), 7.10 (t, J = 16.0 Hz, 2H, Ar-H), 6.96 – 6.89 (m, 2H, Ar-H), 6.11 (s, 2H, CH_2), 2.40 (d, J = 32.0 Hz, 3H, CH_3). MS (ESI): 487.36 (M+H) $^+$. Anal. Calcd for $C_{22}H_{13}F_3N_4O_6$: C, 54.33; H, 2.69; N, 11.52. Found C, 54.31; H, 2.65; N, 11.50.

4.3.3.2-(benzo[*d*][1,3]dioxol-5-yl)-1-(2,6-dinitro-4-(trifluoromethyl)phenyl)-5-fluoro-1*H*-benzo[*d*]imidazole (9a)

Yellow powder, yield 82%. M p: 193-195℃. ^{1}H NMR (400 MHz, DMSO-d_6) δ : 9.07 (S, 2H, Ar-H), 7.82- 7.66 (m, 1H, Ar-H), 7.41 – 7.33 (m, 1H, Ar-H), 7.27 – 7.14 (m, 1H, Ar-H), 7.09 (m, 1H, Ar-H), 7.01 – 6.85 (m, 2H, Ar-H), 6.11 (d, J = 2.8 Hz, 2H, CH_2). MS (ESI): 491.32 (M+H) $^+$. Anal. Calcd for $C_{21}H_{10}F_4N_4O_6$: C, 51.44; H, 2.06; N, 11.43. Found: C, 51.40; H, 2.01; N, 11.41.

4.3.4. 2-(benzo[*d*][1,3]dioxol-5-yl)-5-chloro-1-(2,6-dinitro-4 (trifluoromethyl)phenyl)-1*H*-benzo[*d*]imidazole (9b)

Light yellow powder, yield 83%. M p: 176-178℃. ^{1}H NMR (400 MHz, Chloroform-d_6) δ : 8.49 (s, 2H,Ar-H), 7.86 (d, J =1.2 Hz, 1H, Ar-H), 7.27 (d, J = 8.0 Hz, 1H, Ar-H),7.04 (d, J = 1.6 Hz, 1H, Ar-H), 6.93 – 6.89 (m, 2H, Ar-H), 6.75 (d, J = 8.0 Hz, 1H, Ar-H), 6.02 (s, 2H, CH_2). MS (ESI): 507.78 (M+H) $^+$. Anal. Calcd for $C_{21}H_{10}ClF_3N_4O_6$: C, 49.77; H, 1.99; N, 11.06. Found: C, 49.73; H, 1.96; N, 11.02.

4.3.5.2-(benzo[*d*][1,3]dioxol-5-yl)-5-bromo-1-(2,6-dinitro-4 (trifluoromethyl)phenyl)-1*H*-benzo[*d*]imidazole (10a)

Red powder, yield 81%. M p: 173-175℃. ^{1}H NMR (400 MHz, DMSO-d_6) δ: 9.07 (s, 2H, Ar-H), 7.80-7.70 (s, 1H, Ar-H), 7.49 (ddd, J =15.2, 8.6, 1.8 Hz, 1H, Ar-H),7.34(d, J = 8 Hz, 1H, Ar-H), 7.10 (d, J = 17.4 Hz, 1H, Ar-H), 7.01-6.88 (m, 2H, Ar-H), 6.11 (m, J =2.2 Hz, 2H, CH_2). MS (ESI): 552.23 (M+H) $^+$. Anal. Calcd for $C_{21}H_{10}BrF_3N_4O_6$: C, 45.76; H, 1.83; N, 10.16. Found: C, 45.72; H, 1.81; N, 10.12.

4.3.6.2-(benzo[*d*][1,3]dioxol-5-yl)-1-(2,6-dinitro-4-(trifluoromethyl)phenyl)-5-methoxy-1*H*-benzo[*d*]imidazole (10b)

Red power, yield 29%. M p: 183-185℃. ^{1}H NMR (400 MHz, DMSO-d_6) δ: 9.04 (d, J = 4.4 Hz, 2H, Ar-H), 7.68 (d, J =8.8 Hz, 1H, Ar-H), 7.18(d, J = 8.8 Hz, 1H, Ar-H), 7.09 – 6.88 (m, 4H, Ar-H), 6.10 (d, J = 3.8 Hz, 2H, CH_2), 3.78(d, J = 46.0 Hz, 3H, OCH_3). MS (ESI): 503.36 $(M+H)^+$. Anal. Calcd for $C_{22}H_{13}F_3N_4O_7$: C, 52.60; H, 2.61; N, 11.15. Found: C, 52.58; H, 2.60; N, 11.11.

4.3.7.2-(benzo[*d*][1,3]dioxol-5-yl)-1-(2,6-dinitro-4-(trifluoromethyl)phenyl)-5-(trifluoromethyl)-1*H*-benzo[*d*]imidazole (11a)

Red powder, yield 83%. M p: 187-189℃. ^{1}H NMR (400 MHz, DMSO-d_6) δ: 9.10 (d, J =3.2 Hz ,2H, Ar-H), 8.22 (s, 1H, Ar-H), 7.69 (ddd, J =13.4, 8.68, 1.72 Hz, 1H, Ar-H),7.60(d, J = 8.6 Hz, 1H, Ar-H), 7.13 (d, J = 1.72Hz, 1H, Ar-H), 7.09-6.88 (m, 2H, Ar-H), 6.13 (m, J =2.2 Hz, 2H, CH_2). MS (ESI): 541.33 $(M+H)^+$. Anal. Calcd for $C_{22}H_{10}F_6N_4O_6$: C, 48.90; H, 1.87; N, 10.37. Found: C, 48.88; H, 1.86; N, 10.35.

4.3.8.2-(benzo[*d*][1,3]dioxol-5-yl)-1-(3-chloro-2,6-dinitro-4-(trifluoromethyl)phenyl)-1*H*-benzo[*d*]imidazole (11b)

Red powder, yield 33%. M p: 183-185℃. ^{1}H NMR (400 MHz, Chloroform-d_6) δ: 8.52 (s, 1H, Ar-H) , 7.86 (d, J = 8.0 Hz, 1H, Ar-H), 7.40 (t, J = 7.6 Hz, 1H, Ar-H,), 7.34 – 7.30 (m, 1H, Ar-H), 7.12– 7.10 (m, 2H, Ar-H), 7.00 (d, J = 8.0 Hz, 1H, Ar-H), 6.79 (d, J = 8.0 Hz, 1H, Ar-H),6.03 (d, J = 1.8 Hz, 2H, CH_2). MS (ESI): 507.78 $(M+H)^+$. Anal. Calcd for $C_{21}H_{10}ClF_3N_4O_6$: C, 49.77; H, 1.99; N, 11.06. Found: C, 49.74; H, 1.95; N, 11.02.

4.3.9.2-(benzo[*d*][1,3]dioxol-5-yl)-1-(3-chloro-2,6-dinitro-4-(trifluoromethyl)phenyl)-5-methyl-1*H*-benzo[*d*]imidazole (12a)

Red powder, yield 31%. M p: 163-165℃. ^{1}H NMR (400 MHz, DMSO-d_6) δ: 8.96 (d, J = 5.6 Hz, 1H, Ar-H), 7.73 – 7.54 (m, 1H, Ar-H), 7.31 (d, J = 8.32 Hz, 1H, Ar-H), 7.24 – 7.12 (m, 2H, Ar-H), 7.00 (ddd, J = 8.2, 3.4, 1.92 Hz, 1H, Ar-H), 6.93 (dd, J = 8.2, 1.9 Hz, 1H, Ar-H), 6.12 (s, 2H), 2.41 (d, J = 19.4 Hz, 3H, CH_3). MS (ESI): 521.80 $(M+H)^+$. Anal. Calcd for $C_{22}H_{12}ClF_3N_4O_6$: C, 50.74; H, 2.32; N, 10.76. Found: C, 50.72; H, 2.320; N, 10.74.

4.3.10.2-(benzo[*d*][1,3]dioxol-5-yl)-1-(3-chloro-2,6-dinitro-4-(trifluoromethyl)phenyl)-5-fluoro-1*H*-benzo[*d*]imidazole (12b)

Yellow powder, yield 43%. M p: 173-175℃. ^{1}H NMR (400 MHz, DMSO-d_6) δ : 9.08 (d, J = 3.32 Hz, 1H, Ar-H), 8.06 – 7.86 (m, 2H, Ar-H), 7.50 – 7.41 (m, 1H, Ar-H), 7.25 (d, J = 1.8 Hz, 1H, Ar-H), 7.05 (dd, J = 8.12, 6Hz, 1H, Ar-H), 6.95 (d, J = 8.2Hz, 1H, Ar-H), 6.13 (d, J = 1.68 Hz, 2H, CH_2). MS (ESI): 525.77 $(M+H)^+$. Anal. Calcd for $C_{21}H_9ClF_4N_4O_6$: C, 48.06; H, 1.73; N, 10.68. Found: C, 48.05; H, 1.71; N, 10.66.

4.3.11.2-(benzo[*d*][1,3]dioxol-5-yl)-5-chloro-1-(3-chloro-2,6-dinitro-4-(trifluoromethyl)phenyl)-1*H*-benzo[*d*]imidazole (13a)

Red powder, yield 38%. M p: 174-176℃. ^{1}H NMR (400 MHz, DMSO-d_6) δ: 8.98 (d, J = 3.32 Hz, 1H, Ar-H), 7.97 – 7.66 (m, 2H, Ar-H), 7.45 – 7.34 (m, 1H, Ar-H), 7.20 (d, J = 1.8 Hz, 1H, Ar-H), 7.03 (ddd, J = 8.12, 6.0, 1.8 Hz, 1H, Ar-H), 6.95 (dd, J = 8.2, 1.6 Hz, 1H, Ar-H), 6.13 (d, J = 1.68 Hz, 2H, CH_2). MS (ESI): 542.22 $(M+H)^+$. Anal. Calcd for $C_{21}H_9C_{l2}F_3N_4O_6$: C, 46.60; H, 1.68; N, 10.35. Found: C, 46.55; H, 1.66; N, 10.33.

4.3.12.2-(benzo[*d*][1,3]dioxol-5-yl)-5-bromo-1-(3-chloro-2,6-dinitro-4-(trifluoromethyl)phenyl)-1*H*-benzo[*d*]imidazole (13b)

Red powder, yield 60%. M p: 124-126℃. ^{1}H NMR (400 MHz, Chloroform-d_6) δ: 8.54 (d, J = 8.2 Hz, 1H, Ar-H), 8.00 (d, J = 1.8 Hz, 1H, Ar-H), 7.72 (d, J = 8.6 Hz, 1H, Ar-H), 7.54 – 7.39 (m, 1H, Ar-H), 7.09 (t, J = 2.2 Hz, 1H, Ar-H), 7.04 – 6.94 (m, 1H, Ar-H), 6.79 (d, J = 8.0 Hz, 1H, Ar-H), 6.04 (d, J = 2.2 Hz, 2H, CH_2). MS (ESI): 586.67 $(M+H)^+$. Anal. Calcd for $C_{21}H_9BrClF_3N_4O_6$: C, 43.07; H, 1.55; N, 9.57. Found: C, 43.05; H, 1.52; N, 9.55.

4.3.13.2-(benzo[*d*][1,3]dioxol-5-yl)-1-(3-chloro-2,6-dinitro-4-(trifluoromethyl)phenyl)-5-methoxy-1*H*-benzo[*d*]imidazole (14a)

Red powder, yield 31%. M p: 155-127℃. ^{1}H NMR (400 MHz, DMSO-d_6) δ: 8.95(d, J = 9.8Hz, 1H, Ar-H), 7.33 (d, J =9.4Hz, 1H, Ar-H), 7.15(d, J = 11.88Hz, 1H, Ar-H), 7.08 – 6.84 (m, 4H, Ar-H), 6.11 (d, J = 3.68Hz, 2H, CH_2), 3.79(d, J = 30.6 Hz, 3H, OCH_3). MS (ESI): 537.80 $(M+H)^+$. Anal. Calcd for $C_{22}H_{12}ClF_3N_4O_7$: C, 49.22; H, 2.25; N, 10.44. Found: C, 49.20; H, 2.22; N, 10.41.

4.3.14.2-(benzo[*d*][1,3]dioxol-5-yl)-1-(3-chloro-2,6-dinitro-4-(trifluoromethyl)phenyl)-5-(trifluoromethyl)-1*H*-benzo[*d*]imidazole (14b)

Red powder, yield 28%. M p: 144-146℃. ^{1}H NMR (400 MHz, DMSO-d_6) δ: 9.00 s, 1H, Ar-H), 8.10 – 7.92 (m, 1H, Ar-H), 7.71 (d, J = 10.4 Hz 2H, Ar-H), 7.23 (s, 1H, Ar-H), 7.07 (t, J = 7.6, 1.8 Hz, 1H, Ar-H), 6.96 (d, J = 8.2 Hz, 1H, Ar-H), 6.14(s, 2H, CH_2). MS (ESI): 575.77 $(M+H)^+$. Anal. Calcd for $C_{22}H_9ClF_6N_4O_6$: C, 45.97; H, 1.58; N, 9.75. Found: C, 45.95; H, 1.57; N, 9.74.

4.3.15.2-(2,3-dihydrobenzo[*b*][1,4]dioxin-6-yl)-1-(2,6-dinitro-4-(trifluoromethyl)phenyl)-1*H*-benzo[*d*]imidazole (15a)

Red powder, yield 75%. M p: 164-166℃. ^{1}H NMR (400 MHz, DMSO-d_6) δ : 9.08 (s, 2H, Ar-H), 7.80(d, J = 2.0 Hz 1H, Ar-H), 7.38-7.34 (m, 1H, Ar-H), 7.29 (d, J = 4.0 Hz, 2H, Ar-H), 7.06 (d, J = 2.0 Hz, 1H, Ar-H), 6.94 (dd, J = 2.4, 2.0 Hz, 1H, Ar-H), 6.86 (d, J = 8.4 Hz, 1H, Ar-H), 4.27 (dd, J = 4.8, 5.2 Hz, 4H, CH_2CH_2). MS (ESI): 487.36 $(M+H)^+$. Anal. Calcd for $C_{22}H_{13}F_3N_4O_6$: C, 54.33; H, 2.69; N, 11.52. Found: C, 54.31; H, 2.65; N, 11.50.

4.3.16.2-(2,3-dihydrobenzo[*b*][1,4]dioxin-6-yl)-1-(2,6-dinitro-4-(trifluoromethyl)phenyl)-5-fluoro-1*H*-benzo[*d*]imidazole (16a)

Red powder, yield 78%. M p: 144-146℃. ^{1}H NMR (400 MHz, DMSO-d_6) δ: 9.10 (s, 2H, Ar-H), 7.84-7.81 (m, 1H, Ar-H), 7.39-7.36 (m, 1H, Ar-H), 7.24-7.16 (m, 1H, Ar-H), 7.05 (t, J = 2.0 Hz, 1H, Ar-H), 6.96 – 6.82 (m, 2H, Ar-H), 4.33 – 4.21 (m, 4H, CH_2CH_2). MS (ESI): 505.35 $(M+H)^+$. Anal. Calcd for $C_{22}H_{12}F_4N_4O_6$: C, 52.39; H, 2.40; N, 11.11. Found: C, 52.38; H, 2.39; N, 11.10.

4.3.17.5-chloro-2-(2,3-dihydrobenzo[*b*][1,4]dioxin-6-yl)-1-(2,6-dinitro-4-(trifluoromethyl)phenyl)-1*H*-benzo[*d*]imidazole (16b)

Red powder, yield 88%. M p: 193-195℃. ^{1}H NMR (400 MHz, DMSO-d_6) δ: 9.09 (s, 2H, Ar-H), 7.87 (d, J = 3.2 Hz, 1H, Ar-H), 7.61-7.20 (m, 2H, Ar-H), 7.07 (d, J = 1.6 Hz, 1H, Ar-H), 6.94 (dd, J = 8.0, 1.6 Hz, 1H, Ar-H), 6.88 (t, 1H, Ar-H), 4.39-4.25 (m, 4H, CH_2CH_2). MS (ESI): 521.80 $(M+H)^+$. Anal. Calcd for $C_{22}H_{12}ClF_3N_4O_6$: C, 50.74; H, 2.32; N, 10.76. Found: C, 50.73; H, 2.31; N, 10.74.

4.3.18.5-bromo-2-(2,3-dihydrobenzo[*b*][1,4]dioxin-6-yl)-1-(2,6-dinitro-4-(trifluoromethyl)phenyl)-1*H*-benzo[*d*]imidazole (17a)

Yellow powder, yield 76%. M p: 183-185℃. ^{1}H NMR (400 MHz, DMSO-d_6) δ: 9.10 (d, J = 3.0 Hz, 2H, Ar-H), 8.05 (s, 1H, Ar-H), 7.54 – 7.44 (m, 1H, Ar-H), 7.34 (dd, J = 8.72, 2.2 Hz, 1H, Ar-H), 7.07 (d, J = 5.82 Hz, 1H, Ar-H), 6.98 – 6.83 (m, 2H, Ar-H),4.27(m, 4H, CH_2CH_2). MS (ESI): 566.25 $(M+H)^+$. Anal. Calcd for $C_{22}H_{12}BrF_3N_4O_6$: C, 46.75; H, 2.14; N, 9.91. Found: C, 46.73; H, 2.12; N, 9.90.

4.3.19.2-(2,3-dihydrobenzo[*b*][1,4]dioxin-6-yl)-1-(2,6-dinitro-4-(trifluoromethyl)phenyl)-5-methoxy-1*H*-benzo[*d*]imidazole (17b)

Red powder, yield 58%. M p: 181-183℃. ^{1}H NMR (400 MHz, DMSO-d_6) δ: 9.07 (d, J = 5.2 Hz, 2H, Ar-H), 7.68 (d, J = 8.8 Hz, 1H, Ar-H), 7.18 (d, J = 8.8 Hz, 1H, Ar-H), 7.06 – 6.96 (m, 1H, Ar-H), 6.96 – 6.89 (m, 1H, Ar-H), 6.89 – 6.82 (m, 2H, r-H), 4.30 – 4.23 (m, 4H, CH_2CH_2), 3.77 (d, J = 45.6 Hz, 3H, OCH_3). MS (ESI): 517.35 $(M+H)^+$. Anal. Calcd for $C_{23}H_{15}F_3N_4O_7$: C, 53.50; H, 2.93; N, 10.85. Found: C, 53.47; H, 2.91; N, 10.83.

4.3.20.2-(2,3-dihydrobenzo[*b*][1,4]dioxin-6-yl)-1-(2,6-dinitro-4-(trifluoromethyl)phenyl)-5-(trifluoromethyl)-1*H*-benzo[*d*]imidazole (18a)

Yellow powder, yield 76%. M p: 193-195℃. ^{1}H NMR (400 MHz, DMSO-d_6) δ: 9.12 (s, 2H, Ar-H), 8.01 (d, J = 8.4 Hz, 1H, r-H), 7.92 (s, 1H, Ar-H), 7.70 (d, J = 10.4 Hz, 1H, Ar-H), 7.08 (d, J = 2.2 Hz, 1H, Ar-H), 6.95 (dd, J = 8.6, 2.2 Hz, 1H, Ar-H), 6.88 (d, J = 8.4 Hz, 1H, Ar-H), 4.28 (dd, J = 14.0, 5.2 Hz, 4H, CH_2CH_2). MS (ESI): 555.35 $(M+H)^+$. Anal. Calcd for $C_{23}H_{12}F_6N_4O_6$: C, 49.83; H, 2.18; N, 10.11. Found: C, 49.81; H, 2.17; N, 10.09.

4.3.21.1-(3-chloro-2,6-dinitro-4-(trifluoromethyl)phenyl)-2-(2,3-dihydrobenzo[*b*][1,4]dioxin-6-yl)-1*H*-benzo[*d*]imidazole (18b)

Red powder, yield 48%. M p: 186-188℃. ^{1}H NMR (400 MHz, Chloroform-d_6) δ: 8.57 (s, 1H, Ar-H) ,7.91 (d, J = 8.0 Hz, 1H, Ar-H), 7.44 (t, J = 8.0 Hz, 1H, Ar-H), 7.36 (t, J = 7.8 Hz, 1H, Ar-H), 7.21 (d, J = 2.4 Hz, 1H, Ar-H,), 7.15 (d, J = 8.0 Hz, 1H, Ar-H), 7.00 –7.11 (m, 1H, Ar-H), 6.89 (d, J = 8.4 Hz, 1H, Ar-H), 4.32 (d, J = 8.8 Hz, 4H, CH_2CH_2). MS (ESI): 521.08 $(M+H)^+$. Anal. Calcd for $C_{22}H_{12}ClF_3N4O_6$: C, 50.74; H, 2.32; N, 10.76. Found: C, 50.71; H, 2.31; N, 10.73.

4.3.22.1-(3-chloro-2,6-dinitro-4-(trifluoromethyl)phenyl)-2-(2,3-dihydrobenzo[*b*][1,4]dioxin-6-yl)-5-methyl-1*H*-benzo[*d*]imidazole (19a)

Red powder, yield 58%. M p: 184-186℃. ^{1}H NMR (400 MHz, DMSO-d_6) δ: 8.98 (d, J = 5.2 Hz, 1H, Ar-H), 7.78 – 7.48 (m, 1H, Ar-H), 7.37 – 7.22 (m, 1H, Ar-H), 7.22 – 7.11 (m, 2H, Ar-H), 6.97 (dd, J = 8.4, 2.0 Hz, 1H, Ar-H), 6.88 (d, J = 8.4 Hz, 1H, Ar-H), 4.28 (d, J = 6.0 Hz, 4H, CH_2CH_2), 2.41 (d, J = 7.6 Hz, 3H, CH_3). MS (ESI): 535.83 $(M+H)^+$. Anal. Calcd for $C_{23}H_{14}ClF_3N_4O_6$: C, 51.65; H, 2.64; N, 10.48. Found: C, 51.63; H, 2.62; N, 10.47.

4.3.23.1-(3-chloro-2,6-dinitro-4-(trifluoromethyl)phenyl)-2-(2,3-dihydrobenzo[*b*][1,4]dioxin-6-yl)-5-methoxy-1*H*-benzo[*d*]imidazole (20a)

Red powder, yield 30%. M p: 172-174℃. ^{1}H NMR (400 MHz, DMSO-d_6) δ: 8.97 (d, J = 10.2 Hz, 1H, Ar-H), 7.66 (d, J = 8.8 Hz, 1H, Ar-H), 7.43 – 7.25 (m, 1H, Ar-H), 7.12 (dd, J = 19.2, 2.2 Hz, 1H, Ar-H, 7.00 (dd, J = 11.0, 2.4 Hz, 1H, Ar-H), 6.94 (ddd, J = 12.0, 5.6, 2.4 Hz, 1H, Ar-H), 6.90 – 6.84 (m, 1H, Ar-H), 4.28 (d, J = 8.2 Hz, 4H, CH_2CH_2), 3.79 (d, J = 30.2Hz, 3H, OCH_3). MS (ESI): 551.83 $(M+H)^+$. Anal. Calcd for $C_{23}H_{14}ClF_3N_4O_7$: C, 50.15; H, 2.56; N, 10.17. Found: C, 50.13; H, 2.54; N, 10.16.

4.3.24. 5-bromo-1-(3-chloro-2,6-dinitro-4-(trifluoromethyl) phenyl)-2-(2,3-dihydrobenzo[*b*] [1, 4] dioxin-6-yl)-1*H*-benzo[*d*]imidazole（20b）

Red powder, yield 46%. M p: 180-182℃. ^{1}H NMR (400 MHz, Chloroform-d_6) δ: 8.54 (d, J = 8.4 Hz, 1H, Ar-H), 7.70-7.99 (m, 1H, Ar-H), 7.50-7.41 (m, 1H, Ar-H), 7.16 – 7.11 (m, 1H, r-H), 7.03 – 6.92 (m, 2H, Ar-H), 6.84 (d, J = 8.0 Hz, 1H, r-H), 4.27 (d, J = 8.8 Hz, 4H, CH_2CH_2). MS (ESI): 600.70 $(M+H)^+$. Anal. Calcd for $C_{22}H_{11}BrClF_3N_4O_6$: C, 44.06; H, 1.85; N, 9.34. Found: C, 44.02 H, 1.83; N, 9.31.

4.3.25.1-(3-chloro-2,6-dinitro-4-(trifluoromethyl)phenyl)-2-(2,3-dihydrobenzo[*b*][1,4]dioxin-6-yl)-5-(trifluoromethyl)-1*H*-benzo[*d*]imidazole (21b)

Red powder, yield 32%. M p: 191-193℃. ^{1}H NMR (400 MHz, DMSO-d_6) δ: 9.02 (s, 1H, Ar-H), 8.11 – 7.94 (m, 1H, Ar-H), 7.71 (d, J = 7.6 Hz, 2H, Ar-H), 7.22 (s, 1H, Ar-H), 7.01 (d, J = 6.0, 3.2 Hz, 1H, Ar-H), 6.91 (d, J = 8.4 Hz, 1H, Ar-H), 4.35 – 4.26 (m, 4H, CH_2CH_2). MS (ESI): 589.80 $(M+H)^+$. Anal. Calcd $C_{23}H_{11}ClF_6N_4O_6$: C, 46.92; H, 1.88; N, 9.52. Found: C, 46.90; H, 1.85; N, 9.51.

4.4. Crystal structure determination

Crystal structure determination of compound **8a** was carried out on a Nonius CAD4 diffractometer equipped with graphitemonochromated Mo Ka (k = 0.71073 Å) radiation. The structure was solved by direct methods and refined on F^2 by full-matrix east-squares methods using SHELX-97.32. All the non-hydrogen atoms were refined anisotropically. All the hydrogen atoms were placed in calculated positions and were assigned fixed isotropic thermal parameters at 1.2 times the equivalent isotropic U of the atoms to which they are attached and allowed to ride on their respective parent atoms. The contributions of these hydrogen atoms were included in the structure-factors calculations. The crystal data, data collection and refinement parameters for the compound **8a** were listed in **Table 3**.

4.5. Anti-proliferation assay

The anti-proliferative activities of the prepared compounds against A549, MCF-7 and k562 cells were evaluated as described, elsewhere with some modifications. Generally, target tumor cell lines were grown to log phase in RPMI 1640 medium supplemented with 10% fetal bovine serum, 100 mg/mL streptomycinand 100 IU/mL penicillin. After diluted to 2×10^4 cells mL^{-1} with the complete medium, 100 μL of the obtained cell suspension was added to each well of 96-well culture plates. Following this, the subsequent incubation was then permitted at 37 ℃, 5% CO_2 atmosphere for 24 h before the cytotoxicity assessments.

Tested samples at pre-set concentrations were added to six wells with Colchicine as positive references. After 48 h exposure period, 40 μL PBS containing 2.5 mg mL^{-1} MTT (3-(4,5-dimethylthiazol-2-yl)-2,5-diphenyltetrazolium bromide)) was added to each well. Four hours later, 100 μL DMSO was added and the optical density was measured at a wavelength of 490 nm on an ELISA micro-plate reader. In all experiments three replicate wells were used for each drug concentration. Each assay was carried out for at least three times. The results were summarized in **Table 4**.

4.6. Tubulin polymerization assay

Bovine brain tubulin was purified as described previously. To evaluate the effect of the compounds on tubulin assembly in vitro, varying concentrations of compounds were pre-incubated with 10 μM bovine brain tubulin in glutamate buffer at 30 ℃. And then cooled to 0 ℃. After the addition of 0.4 mM GTP, the mixtures were transferred to 0 ℃ cuvettes in a recording spectrophotometer and warmed up to 30 ℃. Then, the assembly of tubulin was observed turbidimetrically at 350 nm. The IC_{50} was defined as the compound concentration that inhibited the extent of assembly by 50% after 20 min incubation.

4.7. Annexin-V Assay

Surface exposure of PS on apoptotic cells was measured by flow cytometry with a Coulter Cytomics FC500 (Beckman Coulter) by adding annexin-V-FITC to cells according to the manufacturer's instructions (Annexin-V Fluos, Roche Diagnostic). Simultaneously, the cells were stained with PI.

4.8. Flow Cytometric Analysis of Cell Cycle Distribution

For flow cytometric analysis of DNA content, 5×10^5 A549 cells in exponential growth were treated with different concentrations of **18b** for 48 h. After the incubation, the cells were collected, centrifuged, and fixed with ice-cold ethanol (70%). The cells were treated with lysis buffer containing RNase A and 0.1% Triton X-100 and stained with PI. Samples were analyzed on a Cytomic FC500 flow cytometer (Beckman Coulter). DNA histograms were analyzed using ModFit for Windows.

4.9. Experimental protocol of docking study

Molecular docking of compound **18b** into the three dimensional X-ray structure of tubulin (PDB code: 1SA0) was carried out using the Discovery Studio (version 3.5) as implemented through the graphical user interface DS-CDOCKER protocol. The three-dimensional structure of the compound was constructed using Chem. 3D ultra 12.0 software [Chemical Structure Drawing Standard; Cambridge Soft corporation, USA (2010)], then it was energetically minimized by using MMFF94 with 5000 iterations and minimum-RMS gradient of 0.10. The crystal structure of protein complex was retrieved from the RCSB Protein Data Bank (http://www.rcsb.org/pdb/home/home.do). All bound waters and ligands were

eliminated from the protein and the polar hydrogenwas added to the proteins. Molecular docking of all twenty compounds were then carried out using the Discovery Stutio (version 3.5) as implemented through the graphical user interface CDOCKER protocol. CDOCKER is an implementation of a CHARMm based molecular docking tool using a rigid receptor.

4.9.1. 3D-QSAR

Ligand-based 3D-QSAR approach was performed by QSAR software of DS 3.5 (Discovery Studio 3.5, Accelrys, Co. Ltd). The training sets were composed of inhibitors with the corresponding pIC_{50} values which were converted from the obtained IC_{50} (μM), and test sets comprised compounds of data sets. All the definition of the descriptors can be seen in the 'Help' of DS 3.5 software and they were calculated by QSAR protocol of DS 3.5. The alignment conformation of each molecule was the one with lowest interaction energy in the docked results of CDOCKER. The predictive ability of 3D-QSAR modeling can be evaluated based on the cross-validated correlation coefficient, which qualifies the predictive ability of the models. Scrambled test (Y scrambling) was performed to investigate the risk of chance correlations. The inhibitory potencies of compounds were randomly reordered for 30 times and subject to leave-one-out validation test, respectively. The models were also validated by test sets, in which the compounds are not included in the training sets. Usually, one can believe that the modeling is reliable, when the R^2 for test sets is 0.9198.

Acknowledgements

This work was supported by Natural Science Foundation of Jiangsu Province (No. BK20130554) and supported by Major Projects on Control and Rectification of Water Body Pollution (No. 2011ZX07204-001-2214 004).

References and notes

1. A. Frace, C. Loge, S. Gallet, N. Lebegue, P. Carato, P. Chavatte, P. Berthelot and D. J. Lesieur, Enz. Inh. Med. Chem., 2004, 19, 541

2. O. Valiron, N. Caudron and D. Job, Cell. Mol. Life Sci., 2001, 58, 2069.

3. E. Hamel, Med.Chem. Rev., 1996, 16, 207.

4. M. A. Dhamodharan, D. Jordan, L. Thrower and P. Wadsworth, Mol. Biol. Cell, 1995, 6, 1215.

5. J. M. Gerdes and N. Katsanis, Hum. Mol. Genet., 2005, 14, R291.

6. K. P. Singh, R. Rathinasamy and D. Panda, IUBMB Life, 2008, 60, 368.

7. G. M. Chinigo, M. Paige, S. Grindrod, E. Hamel, S. Dakshamamurthy, M. Chruszcz, W. Minor and M. L. Brown, J. Med. Chem., 2008, 51, 4620.

8. R. Romagnoli, P. G. Baraldi, M. D. Carrion, O. Cruz-Lopez, C. L. Cara, G. Basso, G. Viola, M. Khedr, J. Balzarini, S. Mahboobi, A. Sellmer, A. Brancale and E. Hamel, J. Med. Chem., 2009, 52, 5551.

9. K. Nakagawa-Goto, P. C. Wu, C.Y. Lai, E. Hamel, H. Zhu, L. Zhang, T. Kozaka,

E. Ohkoshi, M. Goto, K. F. Bastow, J. Med. Chem., 2011, 54, 1244.

10. R. B. Ravelli, B. Gigant, P. A. Curmi, I. Jourdain, S. Lachkar, A. Sobel and M. Knossow, Nature, 2004, 428, 198.

11. J. L. Hartwell and A. W. Schrecker, Fortschr. Chem. Org. Naturst., 1958, 15, 83.

12. T. F. Imbert, Biochimie, 1998, 80, 207.

13. (a) A. Jordan, J. A. Hadfield, N. J. Lawrence and A. T. McGown, Med. Res. Rev., 1998, 18, 259. (b) K. R. Hande, Etoposide. Eur. J. Cancer, 1998, 34, 1514. (c) P. Meresse, E. Dechaux, C. Monneret and E. Bertounesque, Etoposide. Curr. Med. Chem., 2004, 11, 2443.

14. C. Dumontet and M. A. Jordan, Nat. Rev. Drug Discov., 2010, 9, 790.

15. R. B. Ravelli, B. Gigant, P. A. Curmi, I. Jourdain, S. Lachkar, A. Sobel and M. Knossow, Nature, 2004, 428, 198.

16. A. K. Mukherjee, S. Basu, N. Sarkar and A. C. Ghosh, Curr. Med. Chem., 2001, 8, 1467.

17. A. A. Spasov, I. N. Yozhitsa, L. I. Bugaeva and V. A. Anisimova, Pharm. Chem. J., 1999, 33, 232.

18. K. C. Achar, K. M. Hosamani and H. R. Seetharamareddy, Eur. J. Med. Chem., 2010, 45, 2048.

19. J. Bauer, S. Kinast, A. Burger-Kentischer, D. Finkelmeier, G. Kleymann, W. A. Rayyan, K. Schroppel, A. Singh, G. Jung, K. H. Wiesmuller, S. Rupp and H. J. Eickhoff, Med. Chem. 2011, 54, 6993.

20. B. Garudachari, M. N. Satyanarayana, B. Thippeswamy, C. K. Shivakumar, K. N. Shivananda, G. Hegde and A. M. Isloor, Eur. J. Med. Chem., 2012, 54, 900.

21. C. S. Mizuno, A. G. Chittiboyina, F. H. Shah, A. Patny, T. W. Kurtz, H. A. Pershadsingh, R. C. Speth, V. T. Karamyan, P. B. Carvalho and M. A. Avery, J. Med. Chem., 2010, 53, 1076.

22. R. V. Patel, P. K. Patel, P. Kumari, D. P. Rajani and K. H. Chikhalia, Eur. J. Med. Chem., 2012, 53, 41.

23. K. D. Thomas, A. V. Adhikari, I. H. Chowdhury, E. Sumesh and N. K. Pal, Eur. J. Med. Chem., 2011, 46, 31.

24. C. G. Neochoritis, T. Zarganes-Tzitzikas, C. A. Tsoleridis, J. Stephanidou-Stephanatou, C. A. Kontogiorgis, D. J. Hadjipavlou-Litina and T. Choli-Papadopoulou, Eur. J. Med. Chem., 2011, 46, 297.

25. (a) F. Kallashi, J. Kim, Y. J. Kowalchick, J. A. Park, A. Hunt, C. J. Ali, M. L. Smith, J. V. Hammond, X. Pivnichny, S. S. M. S. Tong, Xu, Y. Anderson, S. S. Chen, Q. Eveland, S. A. Guo, D. P. Hyland, A. M. Milot, M. Curniskey, L. B. Latham, R. Peterson, C. P. Rosa, S. D. Sparrow and P. Sinclair, Bioorg. Med. Chem. Lett., 2011, 21, 172. (b) C. G. Mortimer, J. P. Wells, E. L.Crochard, T. D .Stone, M. F. Bradshaw and A. D. Westwell, J. Med. Chem., 2006, 49, 153.

26. (a) I. N. Stepanenko, A. Casini, F. Edafe, M. S. Novak, V. B. Arion, P. J. Dyson, M. A. Jakupec and B. K. Keppler, Inorg. Chem., 2011, 50, 12669. (b) I. N. Stepanenko, M. S. Novak, G. Muhlgassner, A. Roller, M. Hejl, V. B. Arion, M. A. Jakupec and B. K. Keppler, Inorg. Chem., 2011, 50, 11715. (c) W. Ginzinger, G. Muhlgassner, V. B. Arion, M. A. Jakupec, A. Roller, M. Galanski, M. Reithofer, W. Berger and B. K. Keppler, J. Med. Chem., 2012, 55, 3398.

(d) G. S. Yellol, A. Donaire, J. G. Yellol, V. Vasylyeva, C. Janiak, J. Chem. Commun., 2013, 49, 98.

Figure captions

Figure 1. Chemical structures of antimitotic agents and lead tubulin inhibitors.

Figure 2. Crystal structure diagram of compound **8a**. H atoms are shown as small spheres of arbitrary radii.

Figure 3. Correlation between the anti-proliferative activity against A549 and the tubulin polymerization inhibitory activity, $R^2 = 0.9534$, which indicated that there was a moderate correlation between tubulin polymerization inhibition and inhibition of cellular proliferation.

Figure 4. Representative flow cytometric histograms of apoptotic A549 cells after 24 h treatment with18. The cells were harvested and labeled with Annexin-V-FITC and PI, and then analyzed by flow cytometry.

Figure 5. (A) 2D Ligand interaction diagram of compound **18b** with tubulin using Discovery Studio program with the essential amino acid residues at the binding site are tagged in circles. The purple circles show the amino acids which participate in hydrogen bonding, electrostatic or polar interactions and the green circles show the

amino acids which participate in the Van der Waals interactions. (B) Compound **18b** (colored by atom: carbons: gray; nitrogen: blue; oxygen: red; sulfur: yellow; Bromine: dark red) is bond into tubulin (entry 1SA0 in the Protein Data Bank). The dotted lines show the hydrogen bonds and the yellow line show the pi-action interactions.

Figure 6. The predicted versus experimental pIC_{50} values for the inhibition of tubulin (PDB code: 1SAO).

Figure 7. 3D-QSAR of 1*H*-benzo[*d*]imidazole derivatives for tubulin (PDB code: 1SAO). (A) Isosurface of the 3D-QSAR model coefficients on electrostatic potential grids. The blue triangle mesh represents positive electrostatic potential and the red area represents negative electrostatic potential. (B) Isosurface of the 3D-QSAR model coefficients on Van der Waals grids. The green triangle mesh representation indicates positive coefficients; the yellow triangle mesh indicates negative coefficients.

Scheme 1. Synthesis of compounds **8a-14b**. Reagents and conditions: (i) CH_2Br_2, CH_3CN, 90 ℃, 24 h; K_2CO_3; (ii) DMF, $Na_2S_2O_5$, 110 ℃, 4h; (iii) CH_3CN, K_2CO_3, 100 ℃, 12 h;

Scheme 2. Synthesis of compounds **15a-21b**. Reagents and conditions: (i) $BrCH_2CH_2Br$, CH_3CN, 90 ℃, 24 h; K_2CO_3; (ii) DMF, $Na_2S_2O_5$, 110 ℃, 4 h; (iii) CH_3CN, K_2CO_3 , 100 ℃, 12 h;

Table 1. Structure of compounds **8a–14b**

Table 2. Structure of compounds **15a–21b**

Table 3. Crystallographic and Experimental Data for compound **8a**.

Table 4. *In vitro* cell growth inhibitory effects of compounds **8a-21b** against human tumor cell lines and normal cell line (μM)

Table 5. Interaction energy of compounds **8a-21b**

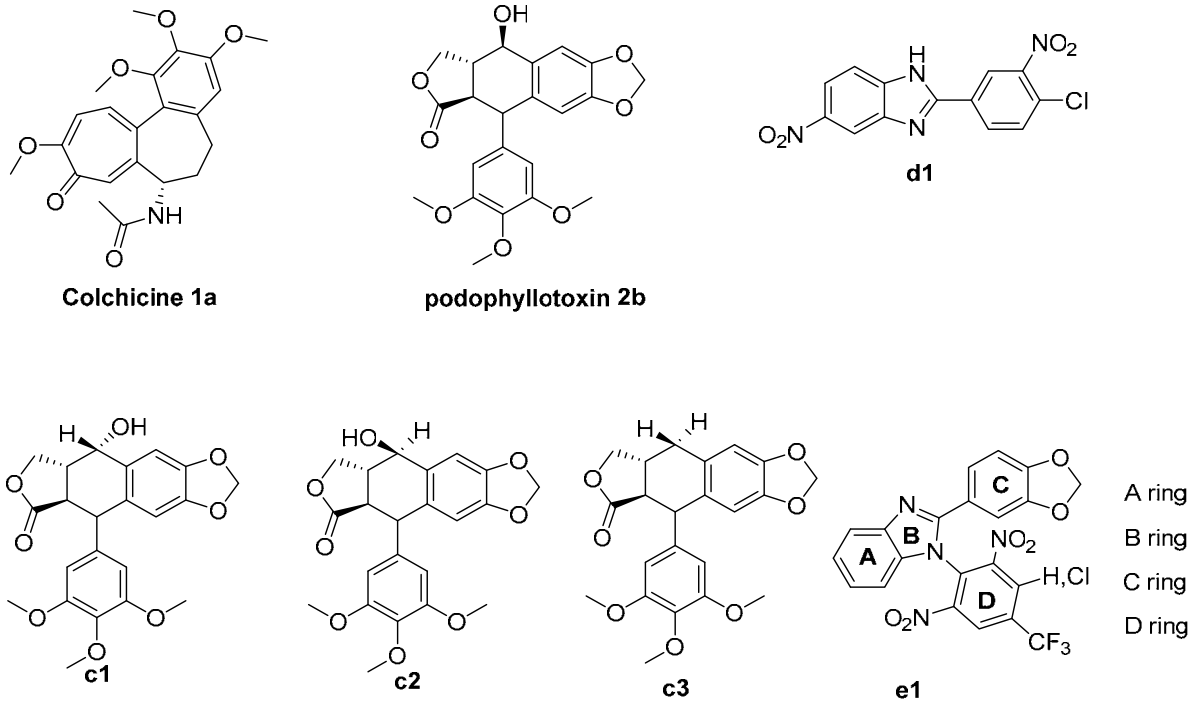

Figure 1. Chemical structures of antimitotic agents and lead tubulin inhibitors.

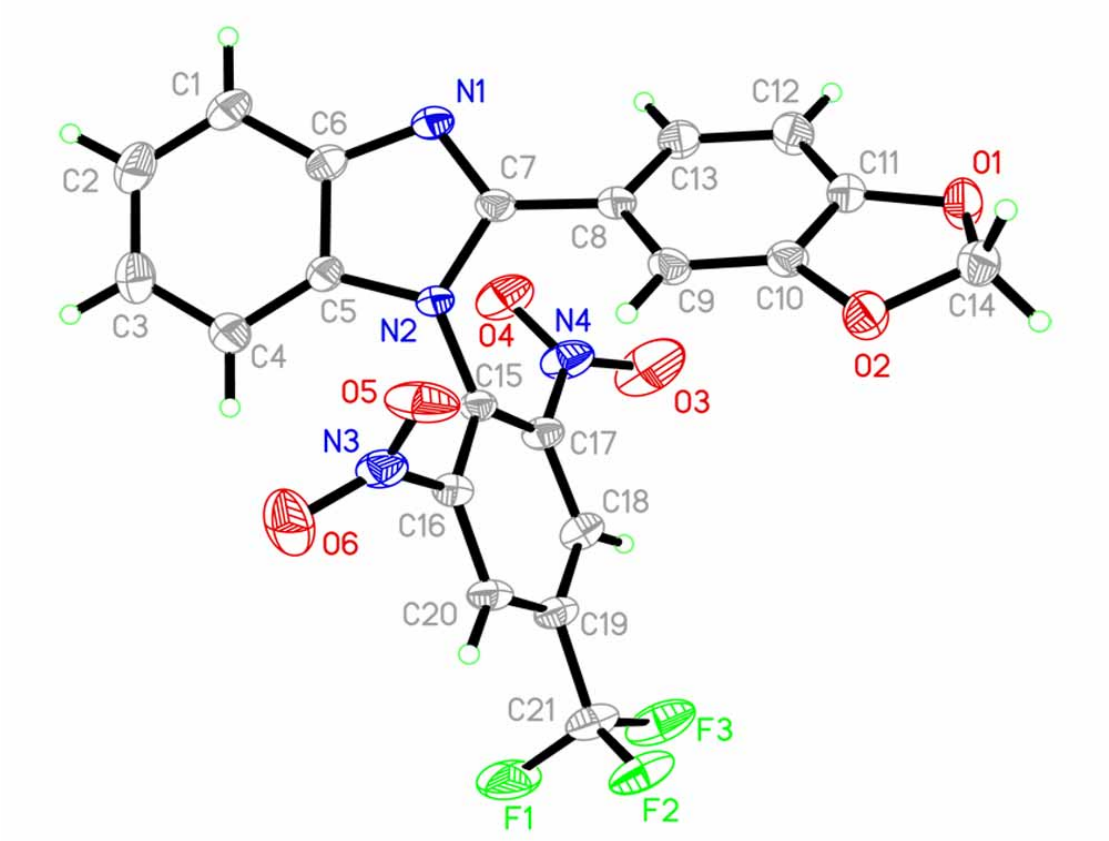

Figure 2. Crystal structure diagram of compound **8a**. H atoms are shown as small spheres of arbitrary radii.

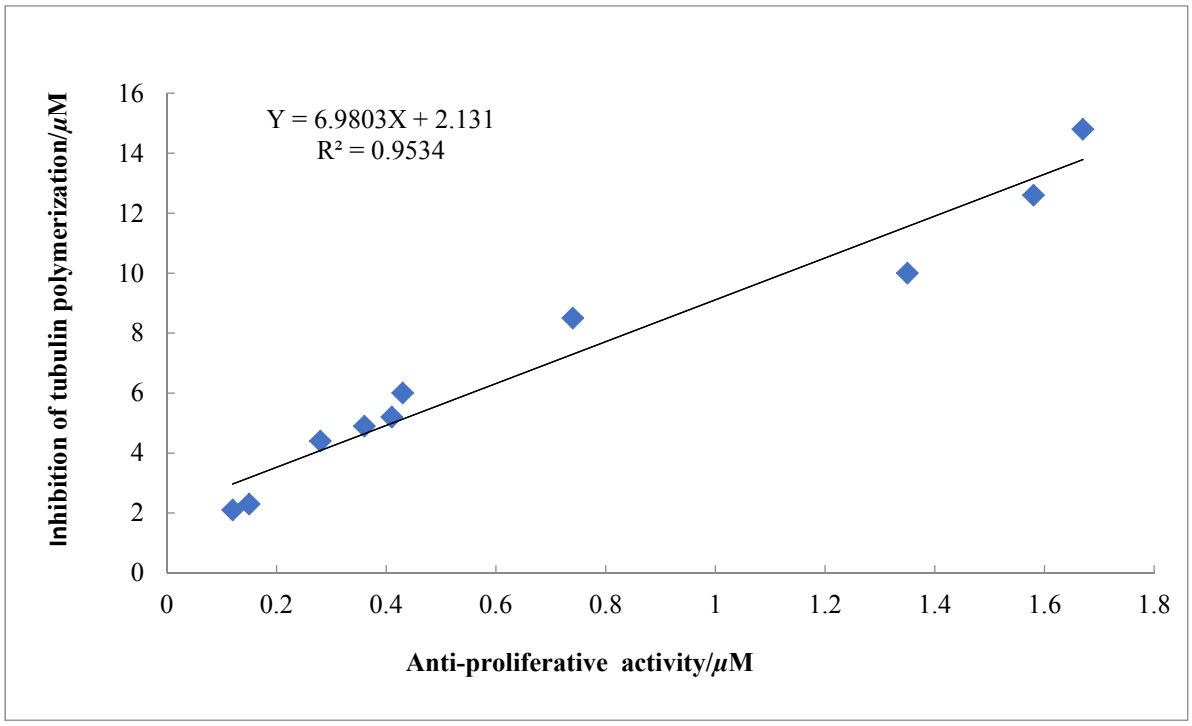

Figure 3. Correlation between the anti-proliferative activity against A549 and the tubulin polymerization inhibitory activity, $R^2 = 0.9534$, which indicated that there was a moderate correlation between tubulin polymerization inhibition and inhibition of cellular proliferation.

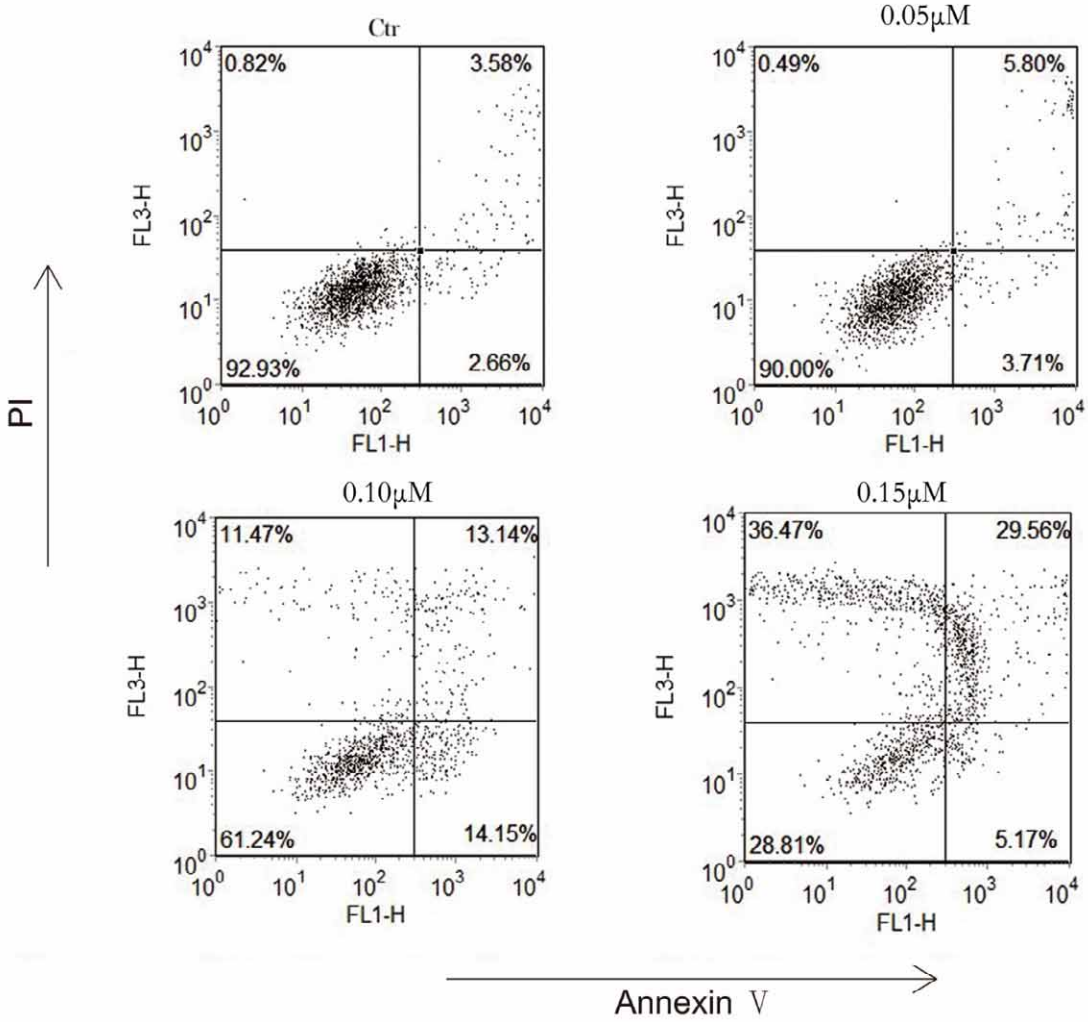

Figure 4. Representative flow cytometric histograms of apoptotic A549 cells after 24 h treatment with compound **18b.** The cells were harvested and labeled with Annexin-V-FITC and PI, and then analyzed by flow cytometry.

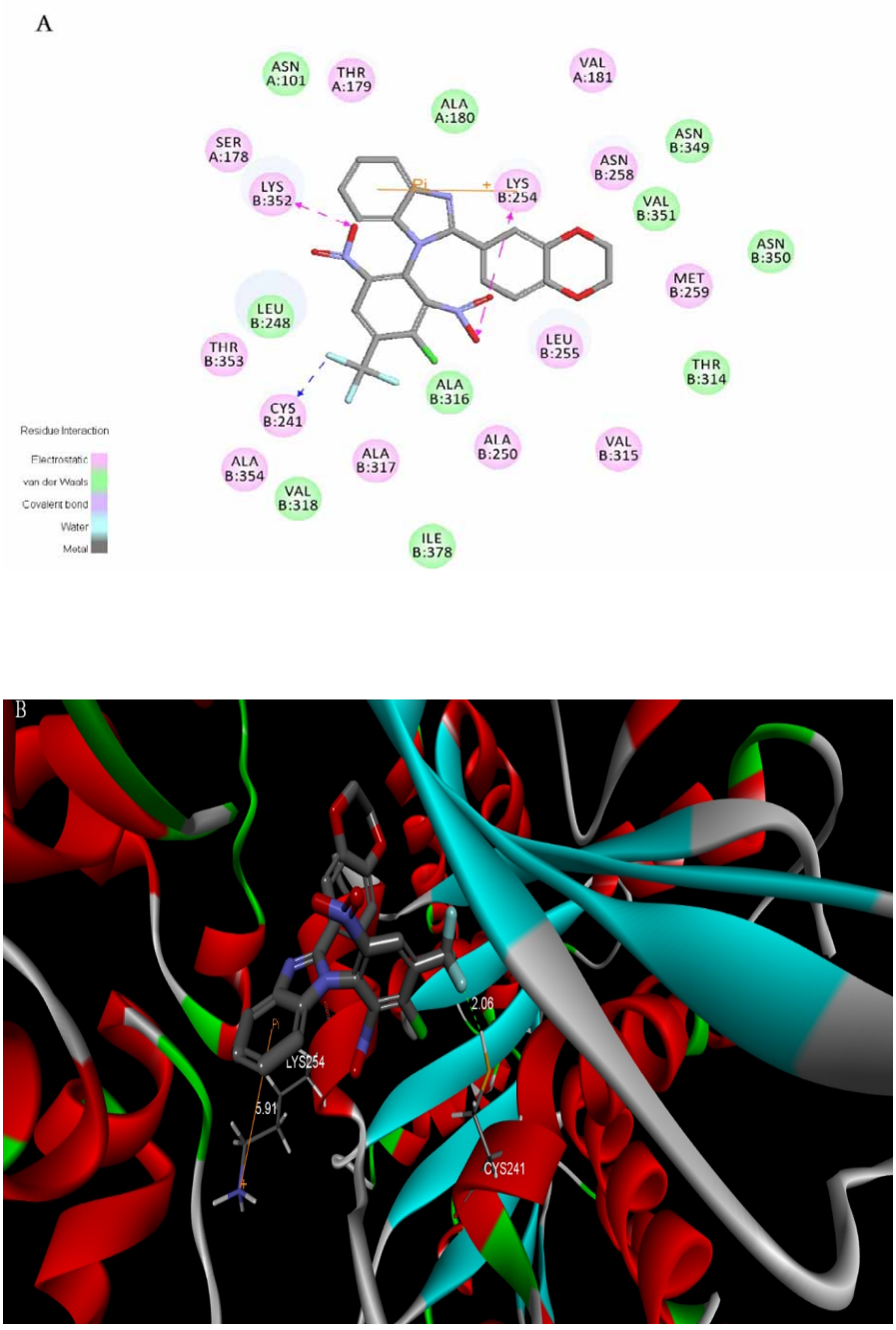

Figure 5. (A) 2D Ligand interaction diagram of compound **18b** with tubulin using Discovery Studio program with the essential amino acid residues at the binding site are tagged in circles. The purple circles show the amino acids which participate in hydrogen bonding, electrostatic or polar interactions and the green circles show the amino acids which participate in the Van der Waals interactions. (B) Compound **18b** (colored by atom: carbons: grey; nitrogen: blue; oxygen: red; sulfur: yellow; Bromine: dark red) is bond into tubulin (entry 1SAO in the Protein Data Bank). The dotted lines show the hydrogen bonds and the yellow line show the pi-action interactions.

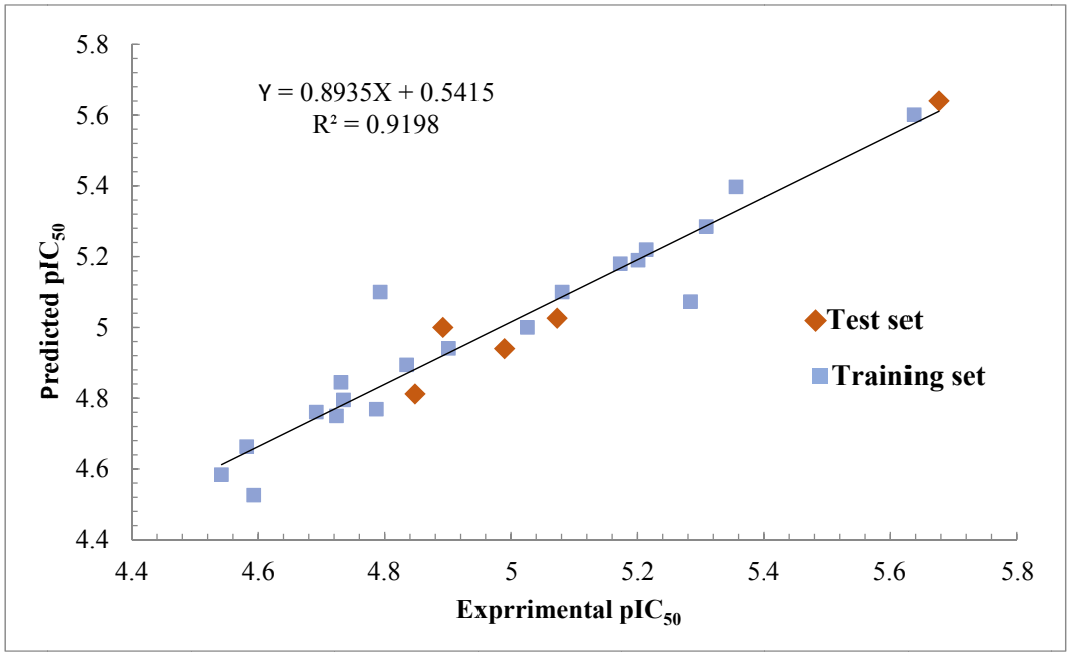

Figure 6. The predicted versus experimental pIC_{50} values for the inhibition of tubulin (PDB code: 1SAO).

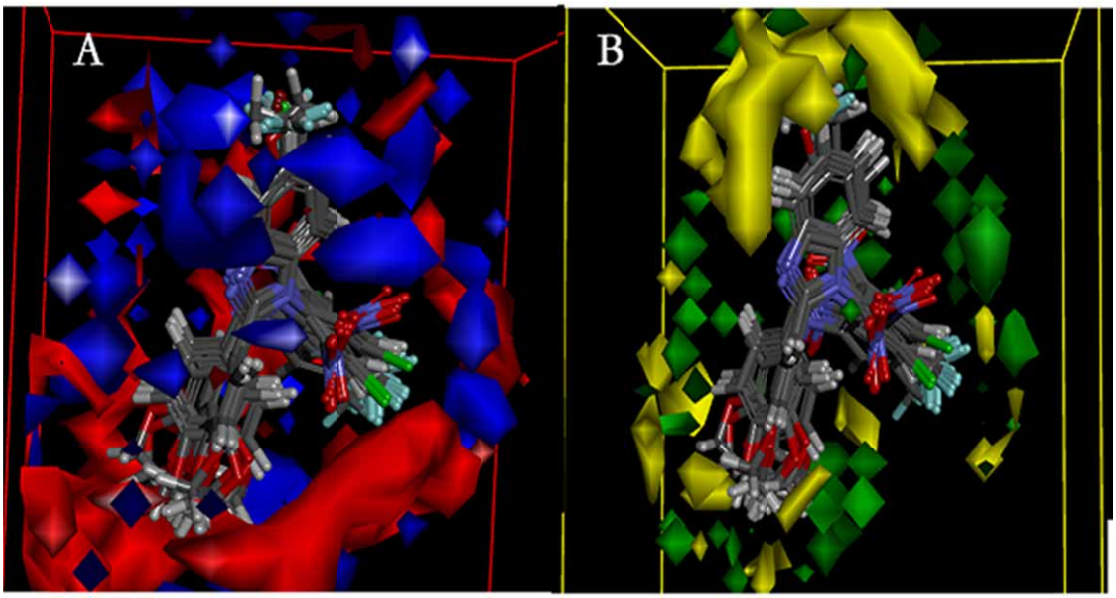

Figure 7. 3D-QSAR of 1*H*-benzo[*d*]imidazole derivatives for tubulin (PDB code: 1SAO). (A) Isosurface of the 3D-QSAR model coefficients on electrostatic potential grids. The blue triangle mesh represents positive electrostatic potential and the red area represents negative electrostatic potential. (B) Isosurface of the 3D-QSAR model coefficients on Van der Waals grids. The green triangle mesh representation indicates positive coefficients; the yellow triangle mesh indicates negative coefficients.

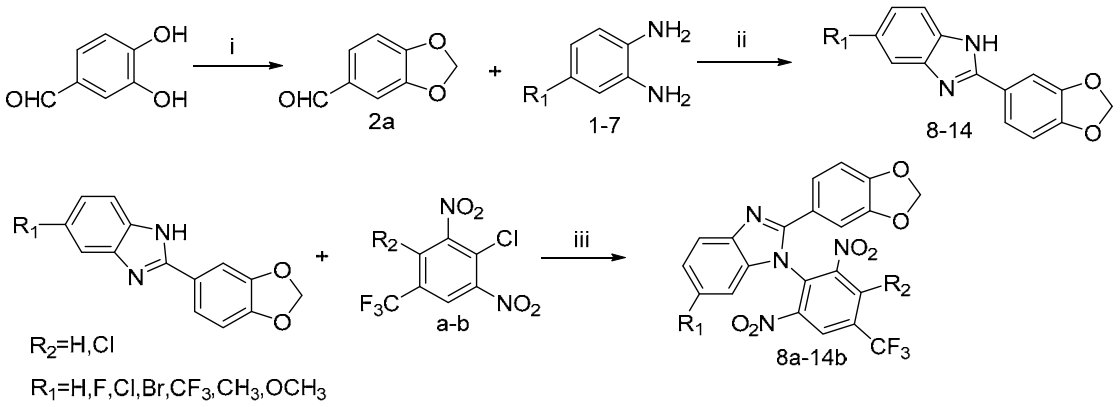

Scheme 1. Synthesis of compounds **8a-14b**. Reagents and conditions: (i) CH_2Br_2, CH_3CN, 90 ℃, 24 h; K_2CO_3; (ii) DMF, $Na_2S_2O_5$, 110 ℃, 4 h; (iii) CH_3CN, K_2CO_3 , 100 ℃, 12 h;

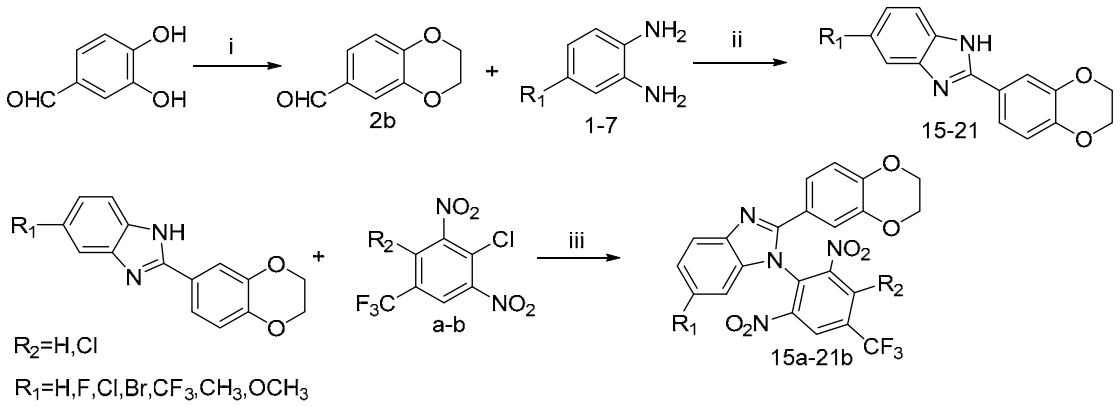

Scheme 2. Synthesis of compounds **15a-21b**. Reagents and conditions: (i) $BrCH_2CH_2Br$, CH_3CN, 90 ℃, 24 h; K_2CO_3; (ii) DMF, $Na_2S_2O_5$, 110 ℃, 4 h; (iii) CH_3CN, K_2CO_3 , 100 ℃, 12 h;

Table 1. Structure of compounds **8a–14b**

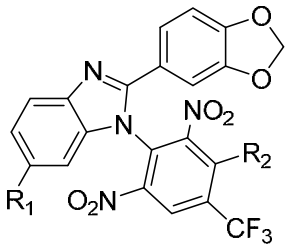

Compound	R_1	R_2
8a	H	H
8b	CH_3	H
9a	F	H
9b	Cl	H
10a	Br	H
10b	OCH_3	H
11a	CF_3	H
11b	H	Cl
12a	CH_3	Cl
12b	F	Cl
13a	Cl	Cl
13b	Br	Cl
14a	OCH_3	Cl
14b	CF_3	Cl

Table 2. Structure of compounds **15a–21b**

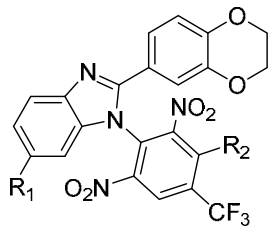

Compound	R_1	R_2
15a	H	H
16a	F	H
16b	Cl	H
17a	Br	H
17b	OCH_3	H
18a	CF_3	H
18b	H	Cl
19a	CH_3	Cl
20a	OCH_3	Cl
20b	Br	Cl
21b	CF_3	Cl

Table 3. Crystallographic and Experimental Data for compound **8a**.

Compound	**8a**
Formula	$C_{21}H_{11}F_3N_4O_6$
Formula weight	472.33
Crystal system	Monoclinic
Space group	*P*21/*n*
a (Å)	8.5592(4)
b (Å)	16.6240(8)
c (Å)	14.1389(6)
α(°)	90.00
β(°)	96.372(2)
γ(°)	90.00
V(Å^3)	1999.37(16)
Z	33
Dc(g•cm^{-3})	1.700
μ(mm^{-1})	0.191
F(000)	1023
θrang(°)	2.66- 27.55
Reflns collected	20400
Reflns unique	4599
Goodness-of-fit on F^2	1.041
R1, wR$_2$[I>2σ(I)]	0.0503, 0.1167
R1, wR$_2$[all data]	0.0819, 0.1338
Max, min$\Delta\rho$(e Å^{-3})	0.414, -0.346

Table 4. *In vitro* cell growth inhibitory effects of compounds **8a-21b** against human tumor cell lines and normal cell line (μM)

Compound	IC_{50}±SD (μM)				CC_{50} (μM)
	A549[a]	MCF-7[a]	K562[a]	Tubulin[b]	293T[d]
8a	0.41±0.07	0.52±0.20	0.34±0.33	5.2±0.12	101.16
8b	11.83±0.09	9.23±0.08	13.35±0.12	26.3±0.09	87.54
9a	2.26±0.04	2.33±0.04	3.46±0.23	8.3±0.21	128.38
9b	4.92±0.12	3.63±0.44	5.41±0.54	12.4±0.32	124.33
10a	5.85±0.13	5.32±0.15	5.72±0.31	19.5±0.11	105.59
10b	6.48±0.42	7.28±0.25	6.49±0.37	25.4±0.42	128.03
11a	7.43±0.21	6.12±0.08	8.41±0.05	31.6±0.23	110.28
11b	0.28±0.03	0.25±0.03	0.32±0.07	4.4±1.11	124.21
12a	8.62±0.14	7.63±0.10	9.74±0.09	6.7±1.41	120.41
12b	1.67±0.21	1.56±0.06	2.32±0.13	14.6±1.16	111.93
13a	2.32±0.08	2.05±0.03	2.71±0.14	12.8±1.23	305.84
13b	3.43±0.23	3.54±0.09	4.31±0.11	14.5±1.22	169.55
14a	8.68±0.45	6.19±0.32	9.43±0.41	18.6±1.41	186.85
14b	6.82±0.26	6.88±0.15	7.92±0.44	20.3±1.56	157.29
15a	0.15±0.02	0.19±0.03	0.31±0.08	2.3±0.15	234.1
16a	0.36±0.08	0.31±0.06	0.54±0.13	4.9±1.32	275.17
16b	0.74±0.11	0.49±0.12	0.82±0.09	8.5±1.26	165.46
17a	1.35±0.03	0.66±0.21	2.15±0.18	9.4±1.13	837.14
17b	2.62±0.23	2.33±0.07	3.63±0.21	16.3±1.31	299.23
18a	3.46±0.22	3.22±0.23	4.56±0.18	18.4±1.32	333.27
18b	0.12±0.03	0.15±0.05	0.21±0.06	2.1±0.06	203.7
19a	3.62±0.06	3.48±0.07	5.38±0.04	16.2±0.45	276.82
20a	0.43±0.19	0.37±0.12	0.62±0.10	6.1±0.12	447.51
20b	1.58±0.22	1.42±0.15	2.84±0.23	12.6±1.22	118.49
21b	2.51±0.13	2.31±0.09	4.37±0.21	6.3±1.01	120.55
Colchicine[c]	0.15±0.02	0.16±0.03	0.28±0.06	2.3±0.11	

[a] Inhibition of the growth of tumor cell lines.

[b] Inhibition of tubulin polymerization.

[c] Used as a positive control.

d Inhibition of the growth of normal cell line.

Table 5. Interaction energy of compounds **8a-21b**

Compound	Interaction energy ΔG_b (kcal / mol))	Compound	Interaction energy ΔG_b (kcal / mol))
8a	-52.7731	**15a**	-60.7260
8b	-48.5859	**15b**	-56.8494
9a	-45.2577	**16a**	-52.7631
9b	-44.3719	**16b**	-49.6707
10a	-43.0285	**17a**	-48.8896
10b	-42.0247	**17b**	-44.0418
11a	-42.6267	**18a**	-41.2035
11b	-55.6741	**18b**	-64.5537
12a	-52.7915	**19a**	-58.8499
12b	-49.7272	**19b**	-55.4261
13a	-48.5123	**20a**	-51.3216
13b	-46.7334	**20b**	-49.5363
14a	-42.3685	**21a**	-45.4679
14b	-43.7368	**21b**	-46.1323